International Journal of Numerical Methods for Heat & Fluid Flow

State estimation in bioheat transfer: a comparison of particle filter algorithms

Bernard Lamien, Leonardo A.B. Varon, Helcio R.B. Orlande, Guillermo E. Elicabe,

State estimation in bioheat transfer: a comparison of particle filter algorithms

Bernard Lamien, Leonardo A.B. Varon and Helcio R.B. Orlande
Department of Mechanical Engineering, Universidade Federal do Rio de Janeiro, Rio de Janeiro, Brazil, and
Guillermo E. Elicabe
Institute of Materials Science and Technology (INTEMA) and National Research Council (CONICET), Universidad Nacional de Mar del Plata, Buenos Aires, Argentina

Received 18 March 2016
Revised 7 May 2016
Accepted 13 May 2016

Abstract

Purpose – The purpose of this paper is to focus on applications related to the hyperthermia treatment of cancer, with heating imposed either by a laser in the near-infrared range or by radiofrequency waves. The particle filter algorithms are compared in terms of computational time and solution accuracy.

Design/methodology/approach – The authors extend the analyses performed in their previous works to compare three different algorithms of the particle filter, as applied to the hyperthermia treatment of cancer. The particle filters examined here are the sampling importance resampling (SIR) algorithm, the auxiliary sampling importance resampling (ASIR) algorithm and Liu & West's algorithm.

Findings – Liu & West's algorithm resulted in the largest computational times. On the other hand, this filter was shown to be capable of dealing with very large uncertainties. In fact, besides the uncertainties in the model parameters, Gaussian noises, similar to those used for the SIR and ASIR filters, were added to the evolution models for the application of Liu & West's filter. For the three filters, the estimated temperatures were in excellent agreement with the exact ones.

Practical implications – This work may help medical doctors in the future to prescribe treatment protocols and also opens the possibility of devising control strategies for the hyperthermia treatment of cancer.

Originality/value – The natural solution to couple the uncertain results from numerical simulations with the measurements that contain uncertainties, aiming at the better prediction of the temperature field of the tissues inside the body, is to formulate the problem in terms of state estimation, as performed in this work.

Keywords Laser heating, Inverse problems, Cancer, Hyperthermia, Particle filters, Radio-frequency heating

Paper type Research paper

Nomenclature

C_p = specific heat;
D = diffusion coefficient for the δ-P1 approximation;
E_0 = maximum laser radiation flux imposed at $z = 0$;
$\mathbf{E}$ = electric field strength;

The financial support provided by FAPERJ, CAPES and CNPq, Brazilian agencies for the fostering of science, is greatly appreciated. The authors also acknowledge the support provided by the STIC AmSud project "I3PE – Inverse Problems in Physical Properties Estimation".

International Journal of Numerical Methods for Heat & Fluid Flow
Vol. 27 No. 3, 2017
pp. 615-638

0961-5539
DOI 10.1108/HFF-03-2016-0118

f = frequency;
g = anisotropy scattering factor;
$\mathbf{H}$ = intensity of the magnetic field;
h = heat transfer coefficient;
k = thermal conductivity;
L_x, L_y = rectangle dimensions in the x and y directions, respectively;
L_r, L_z = radius and thickness of the cylinder, respectively;
n = number of nanoparticles;
N = number of particles for the particle filter;
Q = volumetric heat source
R_1, R_2 = first and second moments of Fresnel's reflection coefficient, respectively;
R_{sc} = specular reflection coefficient at $z = 0$;
r,z = cylindrical coordinates;
T = temperature;
T_∞ = temperature of the surrounding medium;
T_s = initial temperature;
t = time;
U = voltage;
w = weights;
$\mathbf{x}$ = state vector
x,y = Cartesian coordinates; and
$\mathbf{z}$ = vector of measurements.

Greeks

β'_i = reduced total attenuation coefficient of layer i;
β_{tr} = transport attenuation coefficient;
ε = permittivity;
$\boldsymbol{\theta}$ = vector containing all the non-dynamic parameters of the model;
κ = absorption coefficient;
λ = wavelength;
$\pi(a\,|\,b)$ = conditional probability of a when b is given;
ρ = density;
σ = electric conductivity;
σ_s = scattering coefficient;
σ'_s = reduced scattering coefficient;
Φ_p = collimated component of the fluence rate;
Φ_s = diffusive fluence rate;
Φ = total fluence rate;
φ = electric potential;
χ = susceptibility of the magnetic nanoparticles;
Ω' = surface of the rectangular domain;
Ω_1',Ω_2' = boundary patches with electrodes set to voltages U and ground, respectively; and
ω_b = blood perfusion rate.

Superscripts

i = particle index.

Subscripts

1 = healthy tissue;
2 = tumor;
b = blood;
c = cooling;
ext = external heating;
int = internal tissues; and
met = metabolism.

Introduction

The hyperthermia treatment of cancer consists in raising tumor tissues to temperatures between 41-47°C during a pre-specified period. The literature shows an improvement of the efficacy of radiotherapy or chemotherapy when hyperthermia is used as an adjuvant treatment (Hurwitz, 2013; van der Zee, 2002). Among other types of heating, electromagnetic energy sources in the radiofrequency and near-infrared ranges are used to deliver energy to the target region, due to the biological windows of human tissues that exhibit small absorption (Chatterjee and Krishnan, 2013). One major problem of the hyperthermia treatment of cancer is the lack of selectivity of the heating procedure, causing damages to the tumor cells, but to the healthy tissues as well. On the other hand, with the recent advancements in nanotechnology, nanoparticles have been used as absorbing agents in the near-infrared (Bayazitoglu *et al.*, 2013; Hirsch *et al.*, 2003; Huang and El-Sayed, 2010; Khlebtzov and Dykhman, 2010; Rengan *et al.*, 2015; Wang *et al.*, 2012) and in the radiofrequency (Andra *et al.*, 1999; Basel *et al.*, 2012; Bermeo Varon *et al.*, 2015; Gas and Miaskowski, 2015; Gas, 2011; Hergt *et al.*, 2006; Kurgan and Gas, 2009, 2015; Lv *et al.*, 2005; Majchrzak and Paruch, 2011a; Miaskowski and Sawicki, 2013; Murase *et al.*, 2011; Paruch, 2014; Tasci *et al.*, 2009; Varon *et al.*, 2015) ranges.

Numerical simulations are useful tools for planning and/or control of the hyperthermia treatment, but mathematical models depend on several input parameters, including optical, electro-magnetic and thermal properties. These physical properties, as well as the geometry of the tissues, present large variability among individuals, and even for the same individual under different physiological conditions. Therefore, the numerical simulations need to be performed under the effects of uncertainties (Greef *et al.*, 2011; Dos Santos *et al.*, 2009). Meanwhile, techniques for measuring the temperature inside the body have been recently developed, like magnetic resonance (Stafford and Hazle, 2013). Such temperature measurements contain inherent uncertainties. Therefore, within the context of the hyperthermia treatment planning and/or control, numerical simulations of mathematical models containing uncertainties are needed, at the same time that measurements of the temperature inside the body might be available. The natural solution to couple the uncertain results from the numerical simulations with the measurements that contain uncertainties, aiming at the better prediction of the temperature field of the tissues inside the body, is to formulate the problem in terms of state estimation.

In state estimation problems (Andrieu *et al.*, 2004a, 2004b; Arulampalam *et al.*, 2001; Carpenter *et al.*, 1999; Doucet *et al.*, 2000, 2001; Johansen and Doucet, 2008; Kaipio and Fox, 2011; Kaipio *et al.*, 2005; Kaipio and Somersalo, 2004; Kalman, 1960; Liu and Chen, 1998; Maybeck, 1979; Del Moral and Jasra, 2007; Del Moral *et al.*, 2006; Ristic *et al.*, 2004), the available measured data are used together with prior knowledge about the physical phenomena and the measuring devices, to sequentially produce estimates of the desired dynamic variables (temperature distribution in the tissues inside the body, in the present case). State estimation problems are solved within the Bayesian framework, through inference over the posterior distribution of the state variables at each time instant of the problem evolution. Monte Carlo methods have been developed to represent the posterior density in terms of random samples and associated weights. Such Monte Carlo methods, usually denoted as particle filters, can be readily applied to either linear or non-linear models, with Gaussian or non-Gaussian errors (Andrieu *et al.*, 2004a, 2004b; Arulampalam *et al.*, 2001; Carpenter *et al.*, 1999; Doucet *et al.*, 2000, 2001; Johansen and Doucet, 2008; Kaipio *et al.*, 2005; Liu and Chen, 1998; Liu and West, 2001; Del Moral and Jasra, 2007; Del Moral *et al.*, 2006; Orlande *et al.*, 2012; Ristic *et al.*, 2004; Sheinson *et al.*, 2014). The application of particle filters to the solution of inverse problems of state estimation in heat transfer can be found in references (Andrade *et al.*, 2014; Bermeo Varon *et al.*, 2015; Colaço *et al.*, 2012; Lamien *et al.*, 2014, 2015, 2016; Orlande *et al.*, 2012; Silva *et al.*, 2014; Varon *et al.*, 2015; Vianna *et al.*, 2010).

In this paper, we extend the analyses performed in references (Bermeo Varon *et al.*, 2015; Lamien *et al.*, 2014, 2015, 2016; Varon *et al.*, 2015) to compare three different algorithms of the particle filter, as applied to the hyperthermia treatment of cancer. The particle filters examined here are the sampling importance resampling (SIR) algorithm, the auxiliary sampling importance resampling (ASIR) algorithm and Liu & West's algorithm (Andrieu *et al.* 2004a, 2004b; Arulampalam *et al.*, 2001a; Carpenter *et al.*, 1999; Doucet *et al.*, 2000, 2001; Johansen and Doucet, 2008; Liu and Chen, 1998; Liu and West, 2001; Del Moral and Jasra, 2007; Del Moral *et al.*, 2006; Ristic *et al.*, 2004). These algorithms are compared in terms of accuracy and computational time by using simulated transient measurements, in cases involving hyperthermia induced either by a laser in the near-infrared range or by radiofrequency waves. The algorithms used in this paper are presented in the next session, which is followed by the definitions of the hyperthermia problems examined here, by the results obtained with each algorithm and by the conclusions of this work.

State estimation problems

Non-stationary or state estimation inverse problems may be written in the form of evolution and observation models, which are modeled as stochastic processes (Andrieu *et al.* 2004, 2004b; Arulampalam *et al.*, 2001; Carpenter *et al.*, 1999; Doucet *et al.*, 2000, 2001; Johansen and Doucet, 2008; Kaipio and Fox, 2011; Kaipio *et al.*, 2005; Kaipio and Somersalo, 2004; Kalman, 1960; Liu and Chen, 1998; Del Moral and Jasra, 2007; Del Moral *et al.*, 2006). We consider a vector $\mathbf{x}_k$, referred to as the state vector, which contains all the state variables that describe the system at a given time instant t_k. We further assume as known the state evolution model and the observation model, which are defined by the functions $\mathbf{f}_k$ and $\mathbf{g}_k$, respectively, so that we can write (Andrieu *et al.*, 2004a, 2004b; Arulampalam *et al.*, 2001; Carpenter *et al.*, 1999; Doucet *et al.*, 2000, 2001; Johansen and Doucet, 2008; Kaipio and Fox, 2011; Kaipio *et al.*, 2005; Kaipio and Somersalo, 2004; Kalman, 1960; Liu and Chen, 1998; Del Moral and Jasra, 2007; Del Moral *et al.*, 2006):

$$\mathbf{x}_k = \mathbf{f}_k(\mathbf{x}_{k-1}, \boldsymbol{\theta}, \mathbf{v}_k), \; k = 1, \ldots, M \tag{1a}$$

$$\mathbf{z}_k = \mathbf{g}_k(\mathbf{x}_k, \boldsymbol{\theta}, \mathbf{n}_k), \; k = 1, \ldots, M \tag{1b}$$

where $\mathbf{z}_k$ is the prediction of the measurements $\mathbf{z}_k^{meas}$, $\boldsymbol{\theta}$ is a vector containing all the non-dynamic parameters of the model and $\mathbf{v}_k$ and $\mathbf{n}_k$ represent the noises in the state evolution model and in the observation model, respectively. The objective of the state estimation problem is to obtain information about the state vector $\mathbf{x}_k$ based on the evolution and observation models defined by equations (1a) and (1b), with the known probability density $\pi(\mathbf{x}_0,\boldsymbol{\theta}|\mathbf{z}_0) = \pi(\mathbf{x}_0,\boldsymbol{\theta})$ at the initial state $t = t_0$ (Andrieu *et al.* 2004a; 2004b;

Arulampalam *et al.*, 2001; Carpenter *et al.*, 1999; Doucet *et al.*, 2000, 2001; Johansen and Doucet, 2008; Kaipio and Fox, 2011; Kaipio *et al.*, 2005; Kaipio and Somersalo, 2004; Kalman, 1960; Liu and Chen, 1998; Del Moral and Jasra, 2007; Del Moral *et al.*, 2006).

The particle filter method is a Monte Carlo technique for the solution of state estimation problems, in which the posterior probability density function is represented by a set of random samples (particles) with associated weights. We denote $\mathbf{x}_{0:k}^i$, $i = 1, \ldots, N$ the particles with associated weights w_k^i, $i = 1, \ldots, N$ and $\mathbf{x}_{0:k} = \{\mathbf{x}_j, j = 0, \ldots, k\}$ the set of all state variables up to t_k. The weights are normalized so that $\sum_{i=1}^{N} w_k^i = 1$.

The sequential application of the particle filter might result in the degeneracy phenomenon, where after a few states, all but very few particles have negligible weight. The degeneracy implies that a large computational effort is devoted to updating particles whose contribution to the approximation of the posterior density function is almost zero. This problem can be overcome with a resampling step in the application of the particle filter, which deals with the elimination of particles originally with small weights and the replication of particles with large weights (Andrieu *et al.*, 2004a; 2004b; Arulampalam *et al.*, 2001; Carpenter *et al.*, 1999; Doucet *et al.*, 2000, 2001; Johansen and Doucet, 2008; Kaipio *et al.*, 2005; Kaipio and Somersalo, 2004; Liu and Chen, 1998; Del Moral and Jasra, 2007; Del Moral *et al.*, 2006; Ristic *et al.*, 2004). Resampling can be performed if the number of particles with large weights falls below a certain threshold number, or at every instant t_k as in the SIR algorithm (Arulampalam *et al.*, 2001; Ristic *et al.*, 2004). Such an algorithm can be summarized in the following steps, as applied to the system evolution from t_{k-1} to t_k:

Step 1

For $i = 1, \ldots, N$ draw new particles $\mathbf{x}_k^i$ from the prior density $\pi(\mathbf{x}_k|\mathbf{x}_{k-1}^i,\boldsymbol{\theta})$ and then use the likelihood density to calculate the corresponding weights $w_k^i = \pi(\mathbf{z}_k|\mathbf{x}_{k-1}^i,\boldsymbol{\theta})$.

Step 2

Calculate the total weight $T_w = \sum_{i=1}^{N} w_k^i$ and then normalize the particle weights, i.e. for $i = 1, \ldots, N$ let $w_k^i = T_w^{-1} w_k^i$.

Step 3

Resample the particles as follows:
Construct the cumulative sum of weights (CSW) by computing $c_i = c_{i-1} + w_k^i$ for $i = 1, \ldots, N$, with $c_0 = 0$.
Let $i = 1$ and draw a starting point u_1 from the uniform distribution $U[0,N^{-1}]$
For $j = 1, \ldots, N$
  Move along the CSW by making $u_j = u_i + N^{-1}(j-1)$
  While $u_j > c_i$ make $i = i + 1$.
  Assign sample $\mathbf{x}_k^j = \mathbf{x}_k^i$
  Assign sample weight $w_k^j = N^{-1}$

Although the resampling step reduces the effects of degeneracy, it may lead to a loss of diversity and the resultant sample may contain many repeated particles (Andrieu *et al.* 2004a, 2004b; Arulampalam *et al.*, 2001; Carpenter *et al.*, 1999; Doucet *et al.*, 2000, 2001; Johansen and Doucet, 2008; Liu and Chen, 1998; Del Moral and Jasra, 2007; Del Moral *et al.*, 2006; Ristic *et al.*, 2004). An attempt is made to reduce sample impoverishment with the ASIR algorithm, where the resampling step is performed at time t_{k-1} with the available measurements at time t_k (Ristic *et al.*, 2004). The resampling is based on some point estimate $\boldsymbol{\mu}_k^i$ that characterizes $\pi(\mathbf{x}_k^i|\mathbf{x}_{k-1}^i,\boldsymbol{\theta})$, which can be the mean or a sample of $\pi(\mathbf{x}_k^i|\mathbf{x}_{k-1}^i,\boldsymbol{\theta})$. The ASIR algorithm can be summarized in the following steps, as applied to the system evolution from t_{k-1} to t_k (Arulampalam *et al.*, 2001; Ristic *et al.*, 2004):

Step 1

For $i = 1, \ldots, N$ draw new particles $\mathbf{x}_k^i$ from the prior density $\pi(\mathbf{x}_k^i | \mathbf{x}_{k-1}^i, \boldsymbol{\theta})$ and then calculate some characterization $\boldsymbol{\mu}_k^i$ of $\mathbf{x}_k$, given $\mathbf{x}_{k-1}^i$ and $\boldsymbol{\theta}$. Then use the likelihood density to calculate the corresponding weights $w_k^i = (\mathbf{z}_k | \boldsymbol{\mu}_k^i, \boldsymbol{\theta}) w_{k-1}^i$.

Step 2

Calculate the total weight $T = \Sigma_i w_k^i$ and then normalize the particle weights, i.e. for $i = 1, \ldots, N$ let $w_k^i = T^{-1} w_k^i$.

Step 3

Resample the particles as follows:
Construct the cumulative sum of weights (CSW) by computing $c_i = c_{i-1} + w_k^i$ for $i = 1, \ldots, N$, with $c_0 = 0$.
Let $i = 1$ and draw a starting point u_1 from the uniform distribution $U[0, N^{-1}]$
For $j = 1, \ldots, N$
  Move along the CSW by making $u_j = u_1 + N^{-1}(j-1)$
  While $u_j > c_i$ make $i = i + 1$
  Assign sample $\mathbf{x}_k^j = \mathbf{x}_k^i$
  Assign parent $i^j = i$

Step 4

For $j = 1, \ldots, N$ draw particles $\mathbf{x}_k^j$ from the prior density $\pi(\mathbf{x}_k | \mathbf{x}_{k-1}^{ij}, \boldsymbol{\theta})$, using the parent i^j, and then use the likelihood density to calculate the correspondent weights $w_k^j = \pi(\mathbf{z}_k | \mathbf{x}_k^j, \boldsymbol{\theta}) / \pi(\mathbf{z}_k | \boldsymbol{\mu}_k^{ij}, \boldsymbol{\theta})$.

Step 5

Calculate the total weight $T_w = \sum_{j=1}^{N} w_k^j$ and then normalize the particle weights, i.e. for $j = 1, \ldots, N$ let $w_k^j = T_w^{-1} w_k^j$.

The above algorithms of the particle filter relied on deterministic values of the model parameters $\boldsymbol{\theta}$. If these parameters are to be estimated simultaneously with the state variables, one possibility is to apply the SIR or ASIR filters by mimicking the parameters as state variables with an evolution model, for example, in the form of a random walk process, that is:

$$\boldsymbol{\theta}_k = \boldsymbol{\theta}_{k-1} + \mathbf{e}_k \tag{2}$$

where $\mathbf{e}_k$ is a random vector with zero mean and the subscript k for θ is to denote that the parameters will be sequentially estimated together with the state variables; it does not mean that the parameters are time-dependent. Although such an approach can result in accurate estimates for the parameters, even for physically complicated non-linear problems, like in fire propagation (Silva *et al.*, 2014), the simulation of parameters as state variables might fast degenerate the particles (Liu and West, 2001; Sheinson *et al.*, 2014).

On the other hand, the algorithm by Liu and West (2001), which is based on the ASIR version of the particle filter, can be used for the estimation of the posterior probability distribution $\pi(\mathbf{x}_k, \boldsymbol{\theta} | \mathbf{z}_{1:k})$, where $\boldsymbol{\theta}$ represents random parameters of the model. The algorithm of Liu & West for the particle filter is based on West's hypothesis (1993) of a Gaussian mixture for the vector of parameters θ (Rios and Lopes, 2013; West, 1993), that is:

$$\pi(\boldsymbol{\theta} | \mathbf{z}_{1:k-1}) \approx \sum_{i=1}^{N} w_{k-1}^i N(\boldsymbol{\theta} | \mathbf{m}_{k-1}^i, \eta^2 \mathbf{V}_{k-1}) \tag{3}$$

where $N(\cdot|\mathbf{m},\mathbf{S})$ is a Gaussian density with mean $\mathbf{m}$ and covariance matrix $\mathbf{S}$, while η is a smoothing parameter. Equation (3) shows that the density $\pi(\boldsymbol{\theta}|\mathbf{z}_{1:k-1})$ is a mixture of N $(\boldsymbol{\theta}|\mathbf{m}^i_{k-1},\eta^2\mathbf{V}_{k-1})$ distributions weighted by w^i_{k-1}. The kernel locations are specified by using the following shrinkage rule (Liu and West, 2001):

$$\mathbf{m}^i_{k-1} = a\,\boldsymbol{\theta}^i_{k-1} + (1-a)\overline{\boldsymbol{\theta}}_{k-1} \tag{4}$$

where $a = \sqrt{1-\eta^2}$ and $\overline{\boldsymbol{\theta}}_{k-1}$ is the mean of $\boldsymbol{\theta}$ at time t_{k-1}. The shrinkage factor, a, is computed as (Liu and West, 2001):

$$a = \frac{3\delta - 1}{2\delta} \tag{5}$$

where $0.95 < \delta < 0.99$.

The following summarizes the basic steps of Liu & West's algorithm (Liu and West, 2001), as applied for the advancement of the particles from time t_{k-1} to time t_k:

Step 1

Find the mean $\overline{\boldsymbol{\theta}}_{k-1}$ of the parameters $\boldsymbol{\theta}$ at time t_{k-1}.

Step 2

For $i = 1,\ldots,N$ compute $\mathbf{m}^i_{k-1}$ with equation (4), draw new particles $\mathbf{x}^i_k$ from the prior density $\pi(\mathbf{x}^i_k|\mathbf{x}^i_{k-1},\mathbf{m}^i_{k-1})$ and then calculate some characterization $\boldsymbol{\mu}^i_k$ of $\mathbf{x}_k$. Use the likelihood density to calculate the corresponding weights $w^i_k = w^i_{k-1}\pi(\mathbf{z}_k|\boldsymbol{\mu}^i_{k-1},\mathbf{m}^i_{k-1})$.

Step 3

Calculate the total weight $T=\Sigma_i w^i_k$ and then normalize the particle weights, that is, for $i = 1,\ldots,N$ let $w^i_k = T^{-1}w^i_k$.

Step 4

Resample the particles as follows:

Construct the cumulative sum of weights (CSW) by computing $c_i = c_{i-1} + w^i_k$ for $i = 1,\ldots,N$, with $c_0 = 0$

Let $i = 1$ and draw a starting point u_1 from the uniform distribution $U[0,N^{-1}]$

For $j = 1,\ldots,N$

  Move along the CSW by making $u_j = u_1 + N^{-1}(j-1)$

  While $u_j > c_i$ make $i = i + 1$

  Assign samples $\mathbf{x}^j_{k-1} = \mathbf{x}^i_{k-1}$, $\mathbf{m}^j_{k-1} = \mathbf{m}^i_{k-1}$ and $\boldsymbol{\mu}^j_k = \boldsymbol{\mu}^i_k$

  Assign parent $i^j = i$

Step 5

For $j = 1,\ldots,N$ draw samples $\boldsymbol{\theta}^j_k$ from $N(\boldsymbol{\theta}^j_k|\mathbf{m}^{i^j}_{k-1},\eta^2\mathbf{V}_{k-1})$, by using the parent i^j.

Step 6

For $j = 1,\ldots,N$ draw particles $\mathbf{x}^j_k$ from the prior density $\pi(\mathbf{x}_k|\mathbf{x}^{i^j}_{k-1},\boldsymbol{\theta}^j_k)$, using the parent i^j, and then use the likelihood density to calculate the correspondent weights $w^j_k = \pi(\mathbf{z}_k|\mathbf{x}^j_k,\boldsymbol{\theta}^j_k)/\pi(\mathbf{z}_k|\boldsymbol{\mu}^{i^j}_k,\mathbf{m}^{i^j}_{k-1})$.

Step 7

Calculate the total weight $T_w = \sum_{j=1}^{N} w^j_k$ and then normalize the particle weights, that is, for $j = 1,\ldots,N$ let $w^j_k = T_w^{-1}w^j_k$.

Bioheat transfer problems

Two bioheat transfer problems are examined in this work, both related to the hyperthermia treatment of cancer, by using either heating in the near-infrared or radiofrequency ranges (Bermeo Varon *et al.*, 2015; Lamien *et al.*, 2014, 2015, 2016; Varon *et al.*, 2015). There is a variety of models available today for bioheat transfer (Dombrovsky *et al.*, 2011, 2012, 2015; Fan and Wang, 2015; Khaled and Vafai, 2003; Nakayama and Kuwahara, 2008; Pennes, 1948), but none of them was proven as sufficiently general to be applied for different organs or tissues. In fact, even a simple heat conduction model has been recently used for situations similar to those addressed here (Dombrovsky *et al.*, 2015). As the main objective of this work is the comparison of the particle filter algorithms and not model selection, we utilize the classical model proposed by Pennes (1948). The mathematical formulation of the bioheat transfer problem in a domain Ω, with position-dependent thermophysical properties to account for different tissues or organs, and third-kind boundary conditions over the body surface Γ, is given by:

$$\rho(\mathbf{r})c_p(\mathbf{r})\frac{\partial T(\mathbf{r},t)}{\partial t} = \nabla\cdot[k(\mathbf{r})\nabla T(\mathbf{r},t)] + Q(\mathbf{r}),\ \text{in}\ \Omega\,,\ \text{for}\ t>0 \tag{6a}$$

$$k(\mathbf{r})\nabla T(\mathbf{r},t)\cdot\mathbf{n} + h(\mathbf{r})T(\mathbf{r},t) = h(\mathbf{r})T_\infty(\mathbf{r}),\ \text{for}\ \mathbf{r}\in\Gamma,\ t>0 \tag{6b}$$

$$T(\mathbf{r},t) = T_s(\mathbf{r}) \quad \text{in}\ \Omega, t=0 \tag{6c}$$

where $\mathbf{r}$ is the position vector, $\mathbf{n}$ is the unit vector normal to the surface, $h(\mathbf{r})$ is the heat transfer coefficient at the surface of the body, $T_\infty(\mathbf{r})$ is the temperature of the surrounding media and $T_s(\mathbf{r})$ is the initial temperature distribution within the medium, supposed to be the steady-state temperature of the problem when the external heating is null.

The heat source is given by:

$$Q(\mathbf{r}) = \rho_b c_{p,b}\omega_b(\mathbf{r})[T_b - T(\mathbf{r},t)] + Q_{met}(\mathbf{r}) + Q_{ext}(\mathbf{r}) \tag{7}$$

which includes the term resulting from the external heating for the hyperthermia heating, $Q_{ext}(\mathbf{r})$, as well as due to metabolism, $Q_{met}(\mathbf{r})$, and the effect of blood perfusion with a coefficient $\omega_b(\mathbf{r})$.

The problems with heating imposed by a laser in the near-infrared range and by radiofrequency electrodes are now described.

Laser heating

The physical problem examined for this case involves the hyperthermia treatment of a subcutaneous tumor, induced by an external collimated plane laser beam under constant illumination. The skin is represented as an non-homogeneous cylindrical medium with five layers, where each layer corresponds to a specific tissue, namely, epidermis, dermis, fat, muscle and a tumor within the dermis [Figure 1(a)] (Cetingül and Herman, 2010, 2011; Lamien *et al.*, 2016). The tumor is assumed to be loaded with gold nanorods to enhance the hyperthermia effects and to limit such effects to the tumor region. The heat transfer problem resulting from the laser irradiation of the medium is given by Pennes' model in two-dimensional cylindrical coordinates with axial symmetry. The internal surface (at $z = L_z$) is assumed to exchange heat with the deeper tissues with a heat transfer coefficient h_{int}, while the irradiated surface (at $z = 0$) is assumed to be cooled by air to avoid overheating of the skin (Dombrovsky *et al.*, 2012). At the external surface of the skin, at $z = 0$, the heat transfer coefficient and the temperature of the surrounding medium are given, respectively, by h_c and T_c. Heat transfer is neglected through the lateral surfaces of the medium.

The laser radiation propagation in the skin is modeled with the δ-P1 diffusion approximation (Carp *et al.*, 2004; Modest, 2013; Star, 2011). The laser beam is assumed to be co-axial with the cylindrical skin model, so that the problem can be formulated as two-dimensional with axial symmetry. At the external surface of the skin, the incident laser radiation is assumed to be partially reflected (specular reflection), with reflection coefficient R_{sc}. The internal surface of the irradiated boundary is assumed to partially and diffusively reflect the incident radiation, with reflectivity characterized by Fresnel's coefficient A_1, while opacity is assumed for the remaining boundaries. The refractive indexes (n_t) of the different tissues are assumed constant and homogeneous. The mathematical formulation of the radiation problem within the δ-P1 approximation is given by (Star, 2011):

$$\nabla \cdot \left[-D(r,z)\nabla\Phi_s(r,z) + \frac{\sigma_s'(r,z)g'(r,z)}{\beta_{tr}(r,z)}\Phi_p(r,z)\hat{\mathbf{s}}_c \right] + \kappa(r,z)\Phi_s(r,z) = \sigma_s'(r,z)\Phi_p(r,z) \text{ in } 0 < r < L_r \text{ and } 0 < z < L_z \tag{8a}$$

$$-D(r,z)\nabla\Phi_s(r,z)\cdot\mathbf{n} + \frac{1}{2A_1}\Phi_s(r,z) = -\frac{\sigma_s'(r,z)g'(r,z)}{\beta_{tr}(r,z)}\Phi_p(r,z) \ \text{at}\, z = 0,\ 0 < r < L_r \tag{8b}$$

$$\Phi_s(r,z) = 0 \ \text{ at } z = L_z,\ 0 < r < L_r \tag{8c}$$

$$\nabla\Phi_s(r,z)\cdot\mathbf{n} = 0 \ \text{ at } r = 0,\ 0 < z < L_z \tag{8d}$$

$$\Phi_s(r,z) = 0 \ \text{ at } r = L_r,\ 0 < z < L_z \tag{8e}$$

where

$$D = \frac{1}{3\beta_{tr}};\ \sigma_s' = (1-g^2)\sigma_s;\ g' = \frac{g}{1+g};\ A_1 = (1+R_2)/(1-R_1);\ \beta_{tr} = \kappa + \sigma_s(1-g) \tag{9a-e}$$

with g being the anisotropy factor of scattering, σ_S the scattering coefficient and R_1 and R_2 the first and second moments of Fresnel's reflection coefficient, respectively.

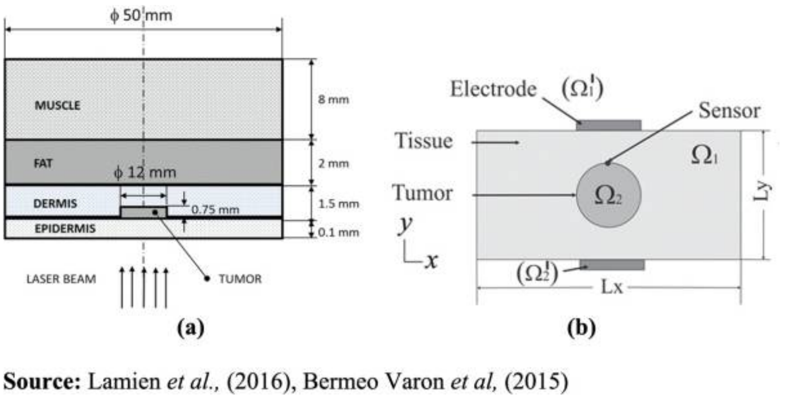

Figure 1. Physical problems for (a) laser heating (Lamien *et al.*, 2016) and (b) radiofrequency heating (Bermeo Varon *et al.*, 2015)

The collimated component of the fluence rate, $\Phi_p(r,z)$, follows the generalized Beer–Lambert's law (Lamien *et al.*, 2014, 2015, 2016) with the imposed laser flux given by:

$$E(r) = \begin{cases} E_0, & r \leq L_{tumor} \\ 0, & r > L_{tumor} \end{cases} \tag{10}$$

where L_{tumor} is the radius of the tumor. The total fluence rate is obtained by adding both diffuse and collimated components, that is:

$$\Phi(r,z) = \Phi_p(r,z) + \Phi_s(r,z) \tag{11}$$

and the heat source term resulting from the laser absorption is given by:

$$Q_{ext}(\mathbf{r}) = \kappa(r,z)\Phi(r,z) \tag{12}$$

Radiofrequency heating

The physical problem considered for radiofrequency heating involves a domain in two dimensions, consisting of a rectangle (healthy tissue) (Ω_1), containing a circular domain (tumor) (Ω_2), as shown by Figure 1(b) (Bermeo Varon *et al.*, 2015). Heating is imposed by radiofrequency waves through the electrodes Ω'_1 and Ω'_2, which are maintained at the voltages U and zero with respect to ground, respectively. The remaining surfaces are electrically insulated. Heat generated inside the domain is propagated by conduction and by blood perfusion, as given by Pennes' model. The top and bottom boundaries exchange heat by convection, where h_c is the heat transfer coefficient and T_c is the temperature of the surrounding medium. The remaining boundaries of the domain are supposed insulated.

The electric potential within the domain can be obtained by solving the following Laplace's equation (Cheng, 1993):

$$\nabla \cdot [\varepsilon(x,y) \cdot \nabla\varphi(x,y)] = 0 \quad x,\, y \in \Omega_1 \cup \Omega_2 \tag{13a}$$

where φ is the potential and ε is the permittivity, which varies spatially depending on the tissue and tumor regions. The boundary conditions for equation (13a) are given by:

$$\varphi(x,y) = U \text{ at } \Omega'_1 \tag{13b}$$

$$\varphi(x,y) = 0 \text{ at } \Omega'_2 \tag{13c}$$

$$\nabla\varphi(x,y) \cdot \mathbf{n} = 0 \text{ else where over the boundary} \tag{13d}$$

After solving problem [equations (13a-13d)], the electric field strength $\mathbf{E}$ can be obtained as:

$$\mathbf{E}(x,y) = -\nabla\varphi(x,y) \tag{14a}$$

and the intensity of the magnetic field $\mathbf{H}$ as:

$$|\mathbf{H}(x,y)| = \frac{1}{1+N(\chi)} \frac{|\mathbf{E}(x,y)|}{\mu_0 \pi f R} \tag{14b}$$

where $N(\chi) = 1/3$ is the demagnetizing factor of the composite tissue (Andra *et al.*, 1999; Lv *et al.*, 2005), χ is the susceptibility of the magnetic nanoparticles that can be described in terms of complex susceptibility, $\chi = \chi' + i\chi''$ (Pankhurst *et al.*, 2003; Rosensweig, 2002), μ_o is the dielectric constant permeability of free space $\mu_o = 4\pi \times 10^{-7}\mathrm{T}\cdot\mathrm{m}\cdot\mathrm{A}^{-1}$, f is the electromagnetic frequency and R is the radius of the magnetic induction loop.

The heat source term in the healthy tissue resulting from the radiofrequency heating is given by:

$$Q_{ext}(\mathbf{r}) = \frac{\sigma_1 |\mathbf{E}(x,y)|^2}{2} \text{ in } \Omega_1 \tag{15a}$$

while in the tumor, the heat source term including the contribution of the magnetic nanoparticles is obtained from (Lv *et al.*, 2005; Majchrzak and Paruch, 2011b):

$$Q_{ext}(\mathbf{r}) = (1-\Theta)\frac{\sigma_2 |\mathbf{E}(x,y)|^2}{2} + \Theta\left[\frac{9}{16}\frac{\chi''}{\mu_0 \pi f R^2}|\mathbf{E}(x,y)|^2\right] \text{ in } \Omega_2 \tag{15b}$$

where $\Theta = n\pi r^2/A$ is the concentration of nanoparticles, r is the mean radius of the supposedly spherical nanoparticles, n is the number of nanoparticles, A is the area of the tumor and σ_2 is the electrical conductivity of the tumor tissue embedded with nanoparticles, which can be approximated by $1/\sigma_2 = (1-\Theta)/\sigma_2' + \Theta/\sigma_3$, where σ_2' and σ_3 are the electrical conductivity of tumor and nanoparticles, respectively (Majchrzak and Paruch, 2011a). The permittivity of the tumor with nanoparticles is approximated by the permittivity of the tumor (Lv *et al.*, 2005).

Results and discussions

The inverse problems that are addressed in this work deal with the estimation of the transient temperature field, for each of the hyperthermia problems described above. The state evolution model for temperature is given by the numerical solution of the bioheat transfer problem given by equation (6), in the domains presented by Figure 1(a) and (b), for laser or radiofrequency heating, respectively. To cope with uncertainties in the temperature evolution model, a Gaussian uncorrelated noise with zero mean and constant standard deviation was added to the solution of equation (6).

For the application of the SIR and ASIR algorithms, uncertainties on the model parameters, $\boldsymbol{\theta}$, were then taken into account through an additive Gaussian noise for the temperature evolution model as described above, as well as through an additive Gaussian noise for the heat source term resulting from the external heating. Therefore, for the application of the SIR and ASIR algorithms, the evolution model for this heat source term, required for the solution of problem (6), was taken in the form of a random walk given by:

$$Q^i_{ext,k}(\mathbf{r}) = Q^i_{ext,k-1}(\mathbf{r}) + \xi^i_k(\mathbf{r}) \tag{16}$$

where i is the particle number and $\xi^i_k(\mathbf{r})$ is a Gaussian random variable with zero mean and a constant standard deviation. The subscript k in equation (16) does not represent a time evolution of $Q_{ext}(\mathbf{r})$, but the fact that it is treated as state variable for the application of the particle filter. The particles $Q^i_{ext,0}(\mathbf{r})$ were initially sampled from Gaussian distributions with means obtained from the deterministic solutions of either problem [equation (8) or (13)], depending on whether the heating was imposed by the laser in the near-infrared range or by the radiofrequency waves, respectively. Thus, in the application of the SIR and ASIR algorithms, the radiation [equation (8)] and electric [equation (13)] problems were decoupled from the bioheat transfer problem [equation (6)], and needed to be solved only once, while the bioheat transfer problem was solved recursively within the filter with the heat source term given by equation (16) for each particle.

For the application of the particle filter of Liu &West, uncertainties in the optical or electrical parameters (depending on the applied heating strategy), as well as uncertainties in the thermal parameters, were given by Gaussian mixtures [see equation (3)]. Therefore, the radiation [equation (8)] and electric [equation (13)] problems were also solved, together with the bioheat transfer problem given by equation (16), at each evolution step of the particle filter.

The state estimation problems were solved by using one single temperature measurement point inside the domain. Uncertainties in such measurements, as well as in the observation model, were taken as Gaussian, additive, uncorrelated, with zero mean and a constant standard deviation.

The performances of the three particle filters analyzed in this work were compared in terms of computational time and accuracy of the estimated temperatures. The root mean square error between the estimated and exact temperatures was used for this purpose, which is given by:

$$RMS = \sqrt{\frac{\sum_{p=1}^{P} (T_{est,p} - T_{exa,p})^2}{P}} \tag{17}$$

where $T_{est,p}$ and $T_{exa,p}$, respectively, represent the estimated and exact temperatures at a position $\mathbf{r}_{i,j}$ and at a time instant t_k, and P is the total number of time steps and locations where the temperatures were compared. The RMS errors are reported in terms of their means and standard deviation values, obtained with 30 runs of each algorithm, to avoid any bias resulting from the simulated measurements. Computational times refer to codes run under the MATLAB platform, on an Intel(R) Xeon E56445@2.40GHz dual processor with 32 GB of RAM memory.

Laser heating

The results presented below were obtained by assuming the optical and thermophysical properties given in Table I for the skin tissues (Bashkatov *et al.*, 2011; Cetingül and Herman, 2010, 2011). However, in the particular case of hyperthermia for which temperature increases do not exceed 10°C, the properties can be assumed constant (Valvano, 2011). We note also that the effects of temperature variation of both thermal and optical properties of skin tissues

Table I.
Thermophysical and optical properties

Tissue	Epidermis	Tumor	Dermis	Fat	Muscle
Thickness (mm)	0.1	0.75	1.5	2	8
ρ (kg/m^3)	1,200	1,030	1,200	1,000	1,085
c_p (J/kg K)	3,589	3,852	3,300	2,674	3,800
k (W/m K)	0.235	0.558	0.445	0.185	0.51
Q_{met} (W/m^3)	0	3680	368.1	368.3	684.2
ω_b (s^{-1})	0	63×10^{-4}	2×10^{-4}	10^{-4}	27×10^{-4}
κ (m^{-1})	35	122	122	108	54
σ_s (m^{-1})	21,270	22,500	22,500	20,200	6,670

Source: Bashkatov *et al.* (2011), Cetingül and Herman (2010, 2011) on the resulting temperature distribution were shown to be insignificant (Quist *et al.*, 2012). Table I also shows the thickness of each layer. The optical properties of the tumor loaded with gold nanorods were calculated with:

$$\kappa_{tot} = \kappa_t + C_{abs} f_v \quad \sigma_{s,tot} = \sigma_s + C_{sca} f_v \tag{18a}$$

by assuming a concentration $f_v = 3 \times 10^{15}$ m^{-3}, where C_{abs} and C_{sca} are the absorption cross-section and the scattering cross-section, respectively. Gold nanorods of effective radius 11.43 nm and aspect ratio 3.9, which have a peak of plasmonic resonance at 797 nm, with $C_{abs} = 2.2128 \times 10^{-14}$ m^2 and $C_{sca} = 1.7286 \times 10^{-15}$ m^2, were used in the simulations (Jain *et al.*, 2006). The calculated absorption and scattering coefficients of the tumor loaded with gold nanorods are 177.02 m^{-1} and 22,503.46 m^{-1}, respectively. It is assumed here that only the absorption and the scattering coefficients are affected by the inclusion of the nanoparticles. The first and second moments of Fresnel's reflection coefficient for the air–tissue interface, with the tissue refractive index $n_t = 1.3$, are given as 0.565 and 0.429, respectively (Prahl, 1988).

For the hyperthermia treatment of the subcutaneous tumor, a collimated plane laser beam was used ($\lambda = 800$ nm, $E_0 = 12$ kW/m^2). The irradiation time was set to 20 s under constant illumination. To avoid overheating of the skin surface, a heat transfer coefficient $h_c = 500$ W/m^{2}K to a medium at $T_c = 35$°C was considered for radial positions smaller than the tumor radius, while the heat transfer coefficient for larger radial positions was set to $h_c = 10$ W/m^{2}K at $T_c = 25$°C (Dombrovsky *et al.*, 2012). The heat transfer coefficient to deeper tissues, supposed to be at the blood temperature of 37°C, was set to $h_{int} = 50$ W/m^{2}K (Dombrovsky *et al.*, 2012). For the solution of both radiation and bioheat transfer problems, a finite volume code based on the alternating direction implicit method was developed and verified (Lamien *et al.*, 2015).

The state estimation problem was solved by assuming transient temperature measurements available from one single sensor located inside the tumor, at $r = 0.5$ mm, $z = 0.7$ mm, taken at a rate of one measurement every 1 s. The measurement errors were assumed Gaussian, with zero mean and a constant standard deviation of 0.5°C. For the application of the SIR and ASIR algorithms, the fluence rate was treated as a state variable with the evolution model in the form of a random walk, with Gaussian noise of zero mean and a standard deviation of 1 per cent of the deterministic value of the fluence rate at each position of the finite volume mesh. A constant standard deviation of 0.5°C was assumed for the evolution model of the temperature. On the other hand, in the case of Liu & West's filter, Gaussian prior probability densities were assumed for the optical and thermophysical properties, with zero means and standard deviations corresponding to approximately 2 per cent of the means (Lamien *et al.*, 2015).

To avoid an inverse crime, different meshes were used for the solution of the forward model for generating the simulated temperature measurements and for state estimation. The state estimation problem was solved with $N = 100$ and $N = 250$ particles. Figure 2(b)-(d) presents the estimated temperature distribution at $t = 20$ s, obtained with the three different filters, for $N = 100$ particles. The exact temperature distribution at $t = 20$ s is presented by Figure 2(a). This figure shows a good agreement between the estimated and exact temperature distributions. The accuracy of the estimated temperatures can also be verified in Figure 3, where the transient variations of the estimated temperatures are compared with the exact ones at the sensor location, for $N = 100$ particles. The simulated transient temperature measurements were also included in these figures. Figures 2 and 3 show that the estimated transient variations of temperature obtained with the three different filters follow the exact

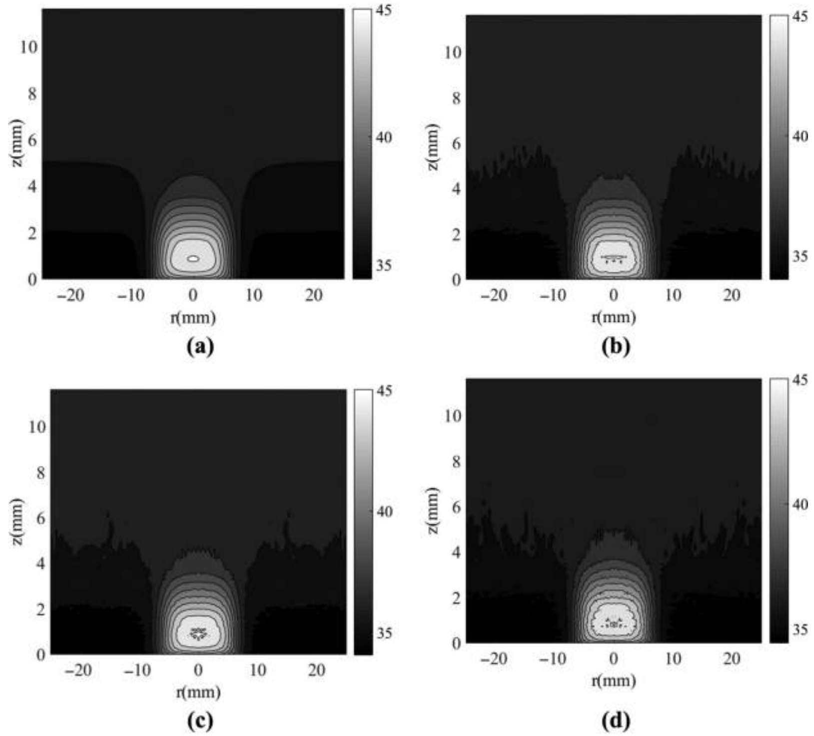

Figure 2.
Comparison of estimated and exact temperature distributions at $t = 20$ s for $N = 100$ particles

Notes: (a) exact; (b) SIR filter; (c) ASIR filter; (d) Liu & West filter

ones, and that the estimated temperatures are generally closer to the exact temperatures than the simulated temperatures.

Table II shows the performance of the SIR, ASIR and Liu & West filters in terms of the computational time, as well as of mean and standard deviation values of the RMS errors of the temperature, for two different number of particles $N = 100$ and $N = 250$. Notice in this table that, as expected, the RMS error is reduced when the number of particles is increased; such is the case for the three particle filter algorithms. Furthermore, it can be noticed that, for the same number of particles, the SIR filter presents the smallest RMS errors, while the largest RMS errors were obtained with Liu & West's filter. Furthermore, the SIR filter generates estimates with the smallest dispersions; thus, the estimates are closer to the exact values for a larger number of runs than for the other filters. Differently than for the SIR and ASIR algorithms, the cases run with Liu & West's algorithm contain uncertainties in the model parameters and in the evolution models; for this reason, the RMS errors of Liu & West's algorithm are the largest. Anyhow, Figures 2 and 3 reveal that the three particle filter algorithms result in accurate estimations of the unknowns for this case, even with a small number of particles such as $N = 100$. The particle filter algorithms were also compared in terms of the computational cost for the state estimation solution. Table II shows the computational time of one run of the SIR, ASIR and Liu & West filters, for $N = 100$ and $N = 250$ particles. It can be noticed in this table that the SIR filter presents the smallest computational cost, while that of the ASIR filter is approximately as twice as that of the SIR

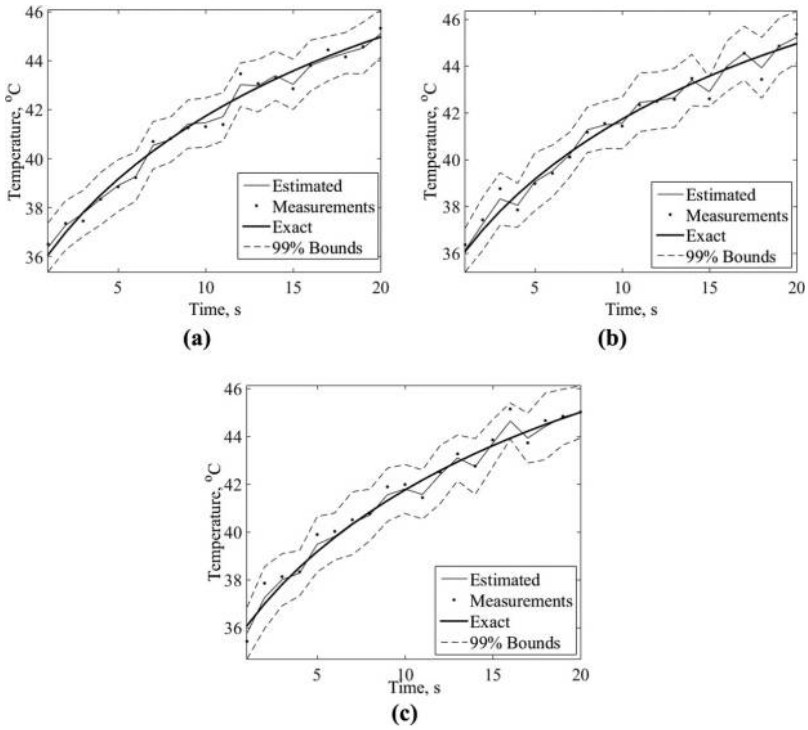

Notes: (a) SIR filter; (b) ASIR filter; (c) Liu & West filter

Figure 3. Comparison of the estimated and exact transient temperature variations with the temperature measurements at the sensor position (r = 0.5 mm, z = 0.7 mm), for N = 100 particles

Filter	No. of particles	RMS error mean (°C)	RMS error standard deviation (°C)	CPU time
SIR	$N = 100$	0.118	0.009	19 min 48 s
	$N = 250$	0.076	0.005	46 min 27 s
ASIR	$N = 100$	0.162	0.021	37 min 49 s
	$N = 250$	0.135	0.026	92 min 50 s
LW	$N = 100$	0.172	0.029	32 h 19 min
	$N = 250$	0.150	0.032	81 h 02 min

Table II. RMS errors of the temperature for laser heating

filter. This is due to the fact that in the ASIR filter, the state evolution is performed twice (see above-mentioned SIR and ASIR algorithms). The computational cost of Liu & West's filter is several times higher than that of the SIR and ASIR filters, as both radiation and bioheat transfer problems need to be solved at each time step for each particle, as discussed above.

Radiofrequency heating

For the case of radiofrequency heating, a 2D rectangular domain of dimensions $L_x = 80$ mm and $L_y = 40$ mm was considered, while the tumor was assumed as a circle of radius $R = 10$ mm located in the center of the 2D rectangular domain. The lengths of both electrodes were considered of 20 mm, so that $\Omega_1' = \{-10 \text{ mm} \leq x \leq 10 \text{ mm}, y = 20 \text{ mm}\}$ and $\Omega_2' =$

$\{-10\,\text{mm} \leq x \leq 10\,\text{mm}, y = -20\,\text{mm}\}$, where the x, y axes are supposed to be located at the tumor center (Figure 2). The voltage applied over Ω_1' was U = 10 V. The following parameters have been assumed: k_1 = 0.5W/mK, k_2 = 0.75W/mK, $c_{p,b} = c_{p,1} = c_{p,2}$ = 4,200 J/kgK, $\rho_b = \rho_1 = \rho_2$ = 1,000 kg/m^3, $\omega_{b,1}$ = 0.0005s^{-1}, $\omega_{b,2}$ = 0.002s^{-1}, T_b = 37°C, $Q_{met,1}$ = 4,200 W/m^3, $Q_{met,2}$ = 42,000 W/m^3, where the subscripts 1, 2 and b denote health tissue, tumor and blood, respectively [Figure 1(b)]. For the convective boundary conditions, we assumed T_c = 20°C, and h_c = 45 W/m^{2}K (Majchrzak and Paruch 2011). For the iron oxide nanoparticles (Fe_3O_4), the following parameters have been considered: k_3 = 40 W/mK, $c_{p,3}$ = 4,000 J/kgK and ρ_3 = 5,180 kg/m^3 (Lv *et al.*, 2005). The properties of the tumor embedded with nanoparticles were approximated by rules of mixtures (Andra *et al.*, 1999; Bermeo Varon *et al.*, 2015). For the electrical parameters in the normal tissue, considering a frequency f = 1 MHz, we used σ_1 = 0.50268 S/m and ε_1 = 1,836.4 (Gabriel *et al.*, 1996), while for the tumor tissue, we have $\sigma_2' = 1.2\sigma_1$ and $\varepsilon_2' = \varepsilon_2 = 1.2\varepsilon_1$ (Majchrzak and Paruch 2011). The electrical properties of the iron oxide nanoparticles were taken as σ_3 = 25,000 S/m and χ'' = 18 (Lv *et al.*, 2005). We assumed for the calculations, a number $n = 10^8$ nanoparticles of radius $r = 10^{-8}$ m. The initial condition for the bioheat transfer problem, which is the solution of the steady-state version of the problem given by equations (6) and (7), for no heat generation from the external RF excitation, i.e. $Q_{ext} = 0$ and h_c = 10 W/m^{2}K at T_c = 25°C (Bermeo Varon *et al.*, 2015). The forward problem, considering the coupled Maxwell's and Penne's equations, was solved with Comsol Multiphysics® 5.0 for this case, while the particle filter algorithms were coded in MATLAB. The forward problem solution for the temperature field at t = 900 s is shown by Figure 4.

Temperature measurements of one single sensor were assumed available for the inverse analysis, located at the position $\{x = 10\,\text{mm}, y = 0\}$. The measurements were generated from the solution of the forward problem with the parameters specified above. Uncorrelated Gaussian errors with zero mean and a constant standard deviation of 1°C were added to the solution of the direct problem. The simulated measurements were supposed available every 20 s, during 900 s. The particle filter algorithms examined in this work were applied with N = 100, 250 and 500 particles.

For the application of the SIR and ASIR algorithms, Gaussian uncorrelated noise with zero mean and a constant standard deviation of 1°C was added to the evolution model for temperature [equation (6)], which was solved with each sample of a Gaussian distribution for the electrical heat source; the means of such Gaussian distribution were obtained from the deterministic solution of the electric problem given by equation (13), with standard deviations given by 10 per cent of these values.

For the application of Liu & West's filter, Gaussian uncorrelated noise with zero mean and a constant standard deviation of 1°C was also added to the solution of the bioheat transfer problem used for the evolution of temperatures. However, differently from the SIR and ASIR filters, the electric problem [equation (13)] was also solved for each particle at each time step

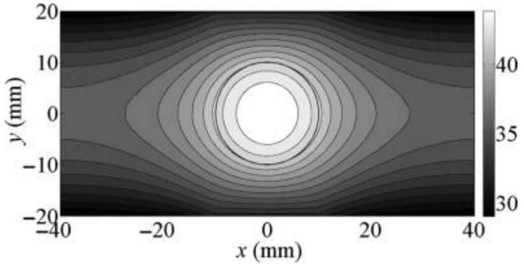

Figure 4.
Exact temperature field

of Liu & West's filter, by considering Gaussian uncertainties in the electric parameters with zero means and standard deviations of 10 per cent of the exact parameter values. The other model parameters were also supposed as Gaussian with means given by their exact values and standard deviations of 10 per cent of their exact values.

Figure 5(a)-(c) presents the estimated temperature fields at $t = 900$ s, obtained with Liu & West's algorithm, by using 100, 250 and 500 particles. Such comparison on the effects of the number of particles on the solution was made with Liu & West's filter because it accounts for uncertainties on the model parameters as well as on the evolution models. Figure 5(a)-(c) shows that, as the number of particles increases, the estimated temperature field tends to the exact one (Figure 4). Therefore, $N = 500$ particles were also used for the results presented by Figure 6(a) and (b), which shows the temperature field in the regions obtained with the SIR and ASIR filters, respectively. A comparison of Figures 4, 5(c) and 6 shows that the temperature field could be accurately estimated with the three filters, despite the large uncertainties in the evolution model, observation model and measurements.

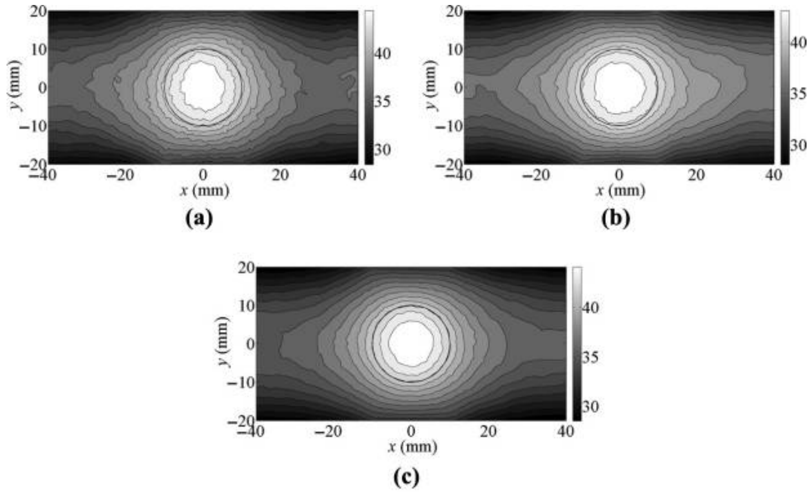

Notes: (a) $N = 100$ particles; (b) $N = 250$ particles; (c) $N = 500$ particles

Figure 5.
Estimated temperature field at $t = 900$ s obtained with Liu & West's filter

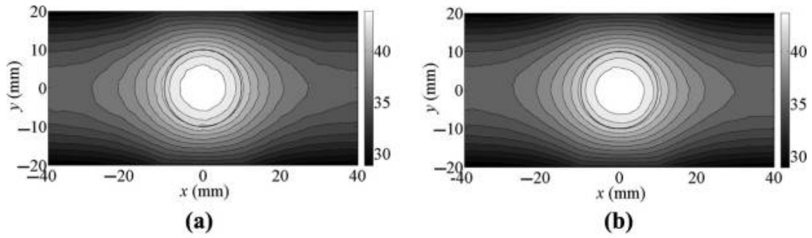

Notes: (a) SIR; (b) ASIR filters

Figure 6.
Estimated temperature fields at $t = 900$ s obtained by using $N =$ 500 particles with

Figure 7(a)-(c) presents the transient temperature variations obtained with the three filters, for $N = 500$ particles, at the measurement position. Such as for the case involving the laser heating, these figures show an excellent agreement between estimated and exact temperatures, with relatively small credible intervals, for the three filters.

The means and the standard deviations of the RMS errors obtained with different numbers of particles for the three filters are presented in Table III. We notice in this table that the SIR and the ASIR filters result in very similar RMS errors, in general smaller than those of the algorithm of Liu & West. This is due to the fact that, in Liu & West's

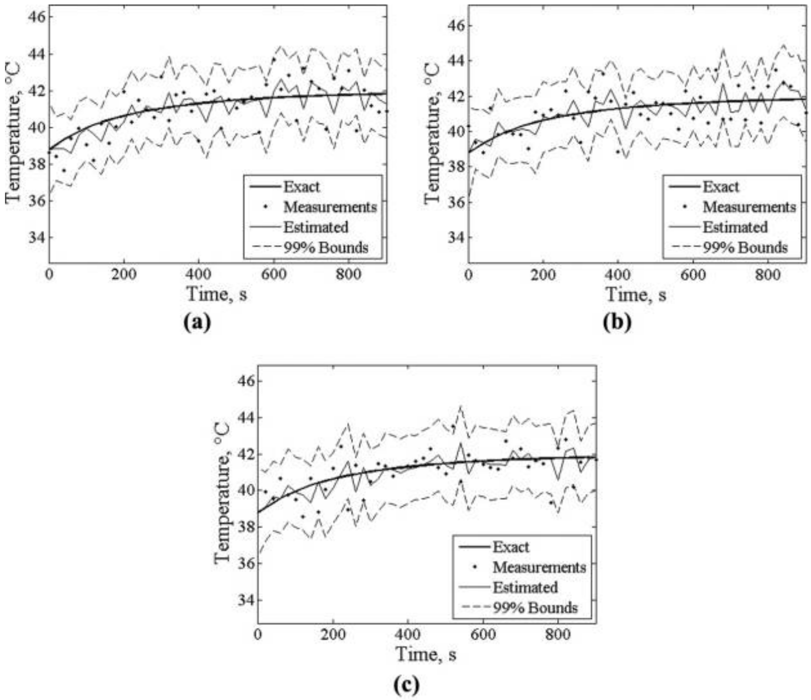

Notes: (a) SIR; (b) ASIR; (c) Liu & West

Figure 7. Estimated at the measurement position $\{x = 10 \text{ mm}, y = 0 \text{ mm}\}$ obtained by using $N = 500$ particles with the algorithms

Table III. RMS errors of the temperature for radiofrequency heating

Filter	No. of particles	RMS error mean (°C)	RMS error standard deviation (°C)	CPU time (h)
SIR	$N = 100$	0.31	0.03	3.9
	$N = 250$	0.25	0.02	9.8
	$N = 500$	0.18	0.02	19.8
ASIR	$N = 100$	0.24	0.04	8.7
	$N = 250$	0.22	0.05	21.7
	$N = 500$	0.15	0.03	43.7
LW	$N = 100$	0.54	0.15	9.1
	$N = 250$	0.32	0.13	22.5
	$N = 500$	0.26	0.12	47.3

algorithm, uncertainties in the model parameters are taken into account in addition to uncertainties in the models. The standard deviations of the RMS errors demonstrate that all algorithms are capable of recovering the exact quantities independently of the set of simulated measurements that were used. Such is the case specially for the SIR algorithm, or when the number of particles is increased. Similar to laser heating, the computational times for the ASIR filter are as twice as those for the SIR filter, with the same number of particles, because the evolution model is computed twice at each time step of the ASIR filter. Besides that, the largest computational times are for Liu & West's algorithm, because the electric and bioheat transfer problems are solved at each time step, during the application of the particle filter.

Conclusions

This paper dealt with the solution of state estimation problems related to the hyperthermia treatment of cancer. Two different heating strategies were considered, by using a laser in the near-infrared range or radiofrequency waves. The objective of the paper was to compare three different algorithms of the particle filter (SIR, ASIR and Liu &West), used for the solution of the state estimation problems with simulated temperature measurements of one single sensor within the domain. The SIR algorithm is one of the simplest implementations of the particle filter, while the ASIR was developed to avoid sample impoverishment, more likely to occur with the SIR algorithm when the noise in the evolution model is small. Liu & West's version of the particle filter was based on the ASIR algorithm, but directly accounts for uncertainties in the model parameters, which are represented as Gaussian mixtures.

In the hyperthermia problems examined in this paper, the bioheat transfer equation was coupled to a radiation transfer problem, in the case of laser heating, or to an electric problem, in the case of radiofrequency heating. Either the radiation transfer or the electric problem provided the external heat source term for the bioheat problem. The SIR and ASIR algorithms were applied with deterministic values of the model parameters and uncertainties in these values were taken into account through the uncertainties in the evolution models. As a result of such an approach, the radiation and electric problems were solved only once to provide the means for the heat source terms, which were modeled as Gaussian. Samples from these Gaussian distributions were then used for the solution of the temperature evolution model, for each particle of the filter. On the other hand, for the application of Liu & West's algorithm, the radiation or the electric problems needed to be solved at each evolution step, because all the parameters were modeled as Gaussian mixtures. Therefore, Liu & West's algorithm resulted in the largest computational times. On the other hand, this filter was shown to be capable of dealing with very large uncertainties. In fact, besides the uncertainties in the model parameters, Gaussian noises, identical to those used for the SIR and ASIR filters, were added to the evolution models for the application of Liu & West's filter. For the three filters, the estimated temperatures were in excellent agreement with the exact ones. For the cases examined above, the SIR algorithm resulted in RMS errors smaller than those of the ASIR algorithm and sample impoverishment was not observed. Therefore, the SIR algorithm is certainly an excellent candidate for practical cases involving actual measured data in the hyperthermia treatment of cancer, because of its simplicity, smaller computational times and stability, even for large uncertainties such as those examined here. The results presented above show that a larger number of particles was needed for larger model and measurement uncertainties.

References

Andra, W., Ambly, C.G., Hergt, R., Hilger, I. and Kaiser, W.A. (1999), "Temperature distribution as function of time around a small spherical heat source of local magnetic hyperthermia", *Journal of Magnetism and Magnetic Materials*, Vol. 194, pp. 197-203.

Andrade, G., Orlande, H.R.B. and Cotta, R. (2014), "Use of particle filter to estimate relative air speed in a Pitot tube", International Symposium on Convective Heat and Mass Transfer – CONV-14, Kusadasi, Turquia.

Andrieu, C., Doucet, A. and Robert, C.P. (2004), "Computational advances for and from Bayesian analysis", *Statistical Science*, Vol. 19 No. 1, pp. 118-127.

Andrieu, C., Doucet, A., Singh, S.S. and Tadic, V.B. (2004), "Particle methods for change detection, system identification, and control", *Proceedings of the IEEE*, Vol. 92 No. 3, pp. 423-438.

Arulampalam, M.S., Maskell, S., Gordon, N. and Clapp, T. (2001), "A tutorial on particle filters for on-line non-linear/non-Gaussian Bayesian tracking", *IEEE Transactions on Signal Processing*, Vol. 50 No. 2, pp. 174-188.

Basel, M.T., Balivada, S., Wang, H., Shrestha, T.B., Seo, G.M., Pyle, M., Abayaweera, G., Dani, R., Koper, O.B., Tamura, M., Chikan, V., Bossmann, S.H. and Troyer, D.L. (2012), "Cell-delivered magnetic nanoparticles caused hyperthermia-mediated increased survival in a murine pancreatic cancer model", *International Journal of Nanomedicine*, Vol. 7, pp. 297-306.

Bashkatov, A.N., Genina, E.A. and Tuchin, V.V. (2011), "Optical properties of skin, subcutaneous, and muscle tissues: a review", *Journal of Innovative Optical Health Sciences*, Vol. 4 No. 1, pp. 9-38.

Bayazitoglu, Y., Kheradmand, S. and Tullius, T.K. (2013), "An overview of nanoparticle assisted laser therapy", *International Journal of Heat and Mass Transfer*, Vol. 67, pp. 469-486.

Bermeo Varon, L.A., Orlande, H.R.B. and Elicabe, G. (2015), "Estimation of state variables in the hyperthermia therapy of cancer with heating imposed by radiofrequency electromagnetic waves", *International Journal of Thermal Sciences*, Vol. 98, pp. 228-236.

Carp, S.A., Prahl, S.A. and Venugopalan, V. (2004), "Radiative transport in the Delta-P1 approximation: accuracy of fluence rate and optical penetration depth predictions in turbid semi-infinite media", *Journal of Biomedical Optics*, Vol. 9 No. 3, pp. 632-647.

Carpenter, J., Clifford, P. and Fearnhead, P. (1999), "An improved particle filter for non-linear problems", *IEE Proceeding – Radar and Sonar Navigation*, Vol. 146 No. 1, pp. 2-7, available at: http://dx.doi.org/10.1049/ip-rsn:19990255

Cetingül, M.P. and Herman, C. (2010), "A heat transfer model of skin tissue for the detection of lesions: sensitivity analysis", *Physics in Medicine and Biology*, Vol. 55 No. 19, pp. 5933-5951.

Çetingül, M.P. and Herman, C. (2011), "Quantification of the thermal signature of a melanoma lesion", *International Journal of Thermal Sciences*, Vol. 50 No. 4, pp. 421-431.

Chatterjee, D. and Krishnan, S. (2013), "Gold nanoparticle – Mediated hyperthermia in cancer therapy", in Cho, S. and Krishnan, S. (Eds), *Cancer Nanotechnology*, CRC Press, Boca Raton, FL.

Cheng, D.K. (1993), *Fundamentals of Engineering Electromagnetics*, Addison-Wesley Publishing Company.

Colaço, M.J., Orlande, H.R.B., B. da Silva, W. and Dulikravich, G.S. (2012), "Application of two Bayesian filters to estimate unknown heat fluxes in a natural convection problem", *Journal of Heat Transfer*, Vol. 134 No. 092501, pp. 1-10.

Del Moral, P., Doucet, A. and Jasra, A. (2006), "Sequential Monte Carlo samplers", *Journal of the Royal Statistical Society: Series B (Statistical Methodology)*, Vol. 68 No. 3, pp. 411-436.

Del Moral, P. and Jasra, A. (2007), "Sequential Monte Carlo for Bayesian Computation", in Bernardo, J.M., Bayarri, M.J., Berger, J.O., Dawid, A.P., Heckerman, D., Smith, A.F.M. and West, M. (Eds), *Bayesian Statistics*, Oxford University, London, pp. 1-34.

Dombrovsky, L.A., Timchenko, V. and Jackson, M. (2012), "Indirect heating strategy for laser induced hyperthermia: an advanced thermal model", *International Journal of Heat and Mass Transfer*, Vol. 55, pp. 4688-4700.

Dombrovsky, L.A., Timchenko, V., Jackson, M. and Yeoh, G.H. (2011), "A Combined Transient Thermal Model for Laser Hyperthermia of Tumors with Embedded Gold Nanoshells", *International Journal of Heat and Mass Transfer*, Vol. 54, pp. 5459-5469.

Dombrovsky, L.A., Timchenko, V., Pathak, C., Piazena, H., Müller, W. and Jackson, M. (2015), "Radiative heating of superficial human tissues with the use of water-filtered infrared-A radiation: a computational modeling", *International Journal of Heat and Mass Transfer*, Vol. 85, pp. 311-320.

Dos Santos, I., Haemmerich, D., Schutt, D., da Rocha, A.F. and Menezes, L.R. (2009), "Probabilistic finite element analysis of radiofrequency liver ablation using the unscented transform", *Physics in Medicine and Biology*, Vol. 54, pp. 627-640.

Doucet, A., Godsill, S. and Andrieu, C. (2000), "On sequential Monte Carlo sampling methods for Bayesian filtering", *Statistics and Computing*, Vol. 10, pp. 197-208.

Doucet, A., Freitas, N. and Gordon, N. (2001), *Sequential Monte Carlo Methods in Practice*, Springer, New York, NY.

Fan, J. and Wang, L. (2015), "Analytical theory of bioheat transport", ICHMT International Symposium on Advances in Computational Heat Transfer, Vol. 1, Piscataway, NJ.

Gabriel, S., Lau, R.W. and Gabriel, C. (1996), "The dielectric properties of biological tissues: III: parametric models for the dielectric spectrum of tissues", *Physics in Medicine and Biology*, Vol. 41 No. 11, pp. 2271-2293.

Gas, P. (2011), "Essential Facts on the History of Hyperthermia and their Connections with Electromedicine", *Przeglad Elektrotechniczny*, Vol. 87 Nos 1/2, pp. 37-40.

Gas, P. and Miaskowski, A. (2015), "Specifying the ferrofluid parameters important from the viewpoint of magnetic fluid hyperthermia", *Selected Problems of Electrical Engineering and Electronics (WZEE)*, available at: http://dx.doi.org/10.1109/WZEE.2015.7394040.

Greef, D.M., Kok, H.P., Correia, D., Borsboom, P.P., Bel, A. and Crezee, J. (2011), "Uncertainty in hyperthermia treatment planning: the need for robust system design", *Physics in Medicine & Biology*, Vol. 56, pp. 3233-3250.

Hergt, R., Dutz, S., Müller, R. and Zeisberger, M. (2006), "Magnetic particle hyperthermia: nanoparticle magnetism and materials development for cancer therapy", *Journal of Physics: Condensed Matter*, Vol. 18 No. 38, pp. S2919-S2934.

Hirsch, L.R., Stafford, R.J., Bankson, J.A, Sershen, S.R., Rivera, B., Price, R.E., Hazle, J.D., Halas, N.J. and West, J.L. (2003), "Nanoshell-mediated near-infrared thermal therapy of tumors under magnetic resonance guidance", *Proceedings of the National Academy of Sciences of the United States of America*, Vol. 100 No. 23, pp. 13549-13554.

Huang, X. and El-Sayed, M.A. (2010), "Gold nanoparticles: optical properties and implementations in cancer diagnosis and photothermal therapy", *Journal of Advanced Research*, Vol. 1 No. 1, pp. 13-28.

Hurwitz, M. (2013), "Principles and application of hyperthermia combined with radiation", in Cho, S. and Krishnan, S. (Eds), *Cancer Nanotechnology*, CRC Press, Boca Raton, FL.

Jain, P.K., Lee, K.S., El-Sayed, I.H. and El-Sayed, M. a. (2006), "Calculated absorption and scattering properties of gold nanoparticles of different size, shape, and composition: applications in biological imaging and biomedicine", *The Journal of Physical Chemistry B*, Vol. 110 No. 14, pp. 7238-7248.

Johansen, A.M. and Doucet, A. (2008), "A note on auxiliary particle filters", *Statistics & Probability Letters*, Vol. 78 No. 12, pp. 1498-1504.

Kaipio, J. and Fox, C. (2011), "The Bayesian framework for inverse problems in heat transfer", *Heat Transfer Engineering*, Vol. 32, pp. 718-753.

Kaipio, J.P. and Somersalo, E. (2004), *Computational and Statistical Methods for Inverse Problems*, Springer, Berlin, Heidelberg.

Kaipio, J.S.D., Seppanen, A., Somersalo, E. and Voutilainen, A. (2005), "State Estimation for Process Imaging", in Scott, D. and McCann, H. (Eds), *Handbook of Process Imaging for Automatic Control*, Boca Raton, FL.

Kalman, R.E. (1960), "A new approach to linear filtering and prediction problems", Vol. 82, pp. 35-45.

Khaled, R.A. and Vafai, K. (2003), "The role of porous media in modeling flow and heat transfer in biological tissues", *International Journal of Heat and Mass Transfer*, Vol. 46 No. 26, pp. 4989-5003.

Khlebtzov, N.G. and Dykhman, L.A. (2010), "Optical properties and biomedical applications of plasmonic nanoparticles", *Journal of Quantitative Spectroscopy and Radiative Transfer*, Vol. 111 No. 1, pp. 1-35.

Kurgan, E. and Gas, P. (2009), "Distribution of the Temperature in Human Body in RF Hyperthermia", *Przeglad Elektrotechniczny*, Vol. 85 No. 12, pp. 96-99.

Kurgan, E. and Gas, P. (2015), "Simulation of the electromagnetic field and temperature distribution in human tissue in RF hyperthermia", *Przeglad Elektrotechniczny*, Vol. 1 No. 1, pp. 171-174.

Lamien, B., Orlande, H.R.B. and Eliçabe, G.E. (2015), "Comparison of particle filter algorithms applied to the temperature filed estimation in hyperthermia phantoms", *1st Thermal and Fluid Engineering Summer Conference, ASTFE, New York, NY*, pp. 1-8.

Lamien, B., Orlande, H.R.B. and Eliçabe, G.E. (2016), "Inverse problem in the hyperthermia therapy of cancer with laser heating and plasmonic nanoparticles", *Inverse Problems in Science and Engineering*, Vol. 25 No. 4.

Lamien, B., Orlande, H.R.B., Elicabe, G.E. and Maurente, A.J. (2014), "State Estimation Problem in Hyperthermia Treatment of Tumors Loaded with Nanoparticles", *Proceedings of the 15th International Heat Transfer Conference, IHTC-15, Kyoto, Japan*, pp. 1-15.

Liu, J. and Chen, R. (1998), "Sequential Monte Carlo methods for dynamical systems", *Journal of American Statistical Association*, Vol. 93, pp. 1032-1044.

Liu, J. and West, M. (2001), "Combined parameter and state estimation in simulation based filtering", *Sequential Monte Carlo Methods in Practice, Part of the Series Statistics for Engineering and Information Science*, pp. 197-217, available at: http://dx.doi.org/10.1007/978-1-4757-3437-9_10.

Lv, Y.-G., Deng, Z.-S. and Liu, J. (2005), "3-D numerical study on the induced heating effects of embedded micro/nanoparticles on human body subject to external medical electromagnetic field", *IEEE Transactions on Nanobioscience*, Vol. 4 No. 4, pp. 284-294.

Majchrzak, E. and Paruch, M. (2011a), "Numerical modelling of the cancer destruction during hyperthermia treatment", *Proceeding: Computer Methods in Mechanics, CMM 2011*, pp. 1-6.

Majchrzak, E. and Paruch, M. (2011b), "Identification of electromagnetic field parameters assuring the cancer destruction during hyperthermia treatment", *Inverse Problems in Science and Engineering*, Vol. 19 No. 1, pp. 45-58.

Maybeck, P. (1979), *Stochastic Models, Estimation, and Control*, Vol. 1, Academic Press, New York, NY.

Miaskowski, A. and Sawicki, B. (2013), "Magnetic fluid hyperthermia modeling based on phantom measurements and realistic breast model", *IEEE Transactions on Bio-Medical Engineering*, Vol. 60 No. 7, pp. 1806-1813.

Modest, M.F. (2013), *Radiative Heat Transfer*, 3rd ed., Academic Press, New York, NY.

Murase, K., Oonoki, J., Takata, H., Song, R., Angraini, A., Ausanai, P. and Matsushita, T. (2011), "Simulation and experimental studies on magnetic hyperthermia with use of superparamagnetic iron oxide nanoparticles", *Radiological Physics and Technology*, Vol. 4 No. 2, pp. 194-202.

Nakayama, A. and Kuwahara, F. (2008), "A general bioheat transfer model based on the theory of porous media", *International Journal of Heat and Mass Transfer*, Vol. 51 No. 11-12, pp. 3190-3199.

Orlande, H., Colaço, M., Dulikravich, G., Vianna, F., Da Silva, W.B., Fonseca, H. and Fudym, O. (2012), "State estimation problems in heat transfer", *International Journal for Uncertainty Quantification*, Vol. 2 No. 3, pp. 239-258.

Pankhurst, Q.A., Connolly, J., Jones, S.K. and Dobson, J. (2003), "Applications of magnetic nanoparticles in biomedicine", *Journal of Physics D: Applied Physics*, Vol. 36 No. 13, pp. R167-R181.

Paruch, M. (2014), "Hyperthermia process control induced by the electric field in order to cancer destroying", *Acta of Bioengineering and Biomechanics*, Vol. 16 No. 4, pp. 123-130.

Pennes, H.H. (1948), "Analysis of tissue and arterial blood temperatures in the resting human forearm. 1948", *Journal of Applied Physiology*, Vol. 1 No. 2, pp. 93-124.

Prahl, S.A. (1988), *Light Transport in Tissue*, The University of Texas, Austin.

Quist, A., Timchenko, V. and Dombrovsky, L.A. (2012), "A simplified model of laser hyperthermia of superficial tumors including variation of human tissue optical properties with thermal damage", *Proceeding of the International Mechanical Engineering Congress & Exposition, IMECE2012, Houston*, pp. 701-709.

Rengan, A.K., Bukhari, A.B., Pradhan, A., Malhotra, R., Banerjee, R., Srivastava, R. and De, A. (2015), "In vivo analysis of biodegradable liposome gold nanoparticles as efficient agents for photothermal therapy of cancer", *Nano Lett*, Vol. 15 No. 2, pp. 842-848.

Rios, M.P. and Lopes, H.F. (2013), "The extended liu and west filter: parameter learning in markov switching stochastic volatility models", in Zeng, Y. and S. Wu (Eds), *State-Space Models: Applications in Economics and Finance, Statistics and Econometrics for Finance*, Vol. 1, New York, NY, pp. 23-62.

Ristic, B., Arulampalam, M.S. and Gordon, N. (2004), *Beyond the Kalman Filter*, Artech House, Boston, MA.

Rosensweig, R.E. (2002), "Heating magnetic fluid with alternating magnetic field", *Journal of Magnetism and Magnetic Materials*, Vol. 252, pp. 370-374.

Sheinson, D.M., Niemi, J. and Meiring, W. (2014), "Comparison of the performance of particle filter algorithms applied to tracking of a disease epidemic", *Mathematical Biosciences*, Vol. 255, pp. 21-32.

Silva, W.B., Rochoux, M., Orlande, H.R.B., Colaço, M.J., Fudym, O., Hafi, M. , Cuenot, B. and Ricci, S. (2014), "Application of particle filters to regional-scale wildfire spread", *High Temperatures. High Pressures*, Vol. 43 No. 6, pp. 435-440.

Stafford, R. and Hazle, J. (2013), "Magnetic resonance temperature imaging for gold nanoparticle-mediated thermal therapy", in Cho, S. and Krishnan, S. (Eds), *Cancer Nanotechnology*, CRC Press, Boca Raton, FL.

Star, W.M. (2011), "Diffusion theory of light transport", in Welch, A.J. and Van Gemert, J.C.M. (Eds), *Optical-Thermal Response of Laser Irradiated Tissue*, 2nd ed., Springer, New York, NY.

Tasci, T.O., Vargel, I., Arat, A., Guzel, E., Korkusuz, P. and Atalar, E. (2009), "Focused RF hyperthermia using magnetic fluids", *Med Phys.*, Vol. 36 No. 5, pp. 1906-1912.

Valvano, J.W. (2011), "Tissue thermal properties and perfusion", in Van Gemert, J.C.M. (Ed.), *Optical-Thermal Response of Laser Irradiated Tissue*, Springer, Dordrecht Heidelberg London; New York, NY.

van der Zee, J. (2002), "Heating the patient: a promising approach?", *Annals of Oncology*, Vol. 13 No. 8, pp. 1173-1184.

Varon, L.A.B., Orlande, H.R.B. and Elicabe, G.E. (2015), "State estimation problem with particle filter for the radiofrequency hyperthermia therapy combined with nanoparticles", *1st Thermal and Fluid Engineering Summer Conference, ASTFE, New York*, pp. 1-8, available at: http://dx.doi.org/10.1615/TFESC1.bio.013638

Vianna, F.L.V., Orlande, H. and Dulikravich, G. (2010), "Temperature Field Prediction of a Multilayered Composite Pipeline Based on the Particle Filter Method", *Heat Transfer. Eng.* Vol. 2, pp. 1-10.

Wang, Q., Xie, L., He, Z., Di, D. and Liu, J. (2012), "Biodegradable magnesium nanoparticle-enhanced laser hyperthermia therapy", *International Journal of Nanomedicine*, Vol. 7, pp. 4715-4725.

West, M. (1993), "Approximating posterior distributions by mixture", *Journal of the Royal Statistical Society B*, No. 55, pp. 409-422.

Corresponding author
Helcio R.B. Orlande can be contacted at: helcio@mecanica.coppe.ufrj.br